Preprints of the 19th World Congress
The International Federation of Automatic Control
Cape Town, South Africa. August 24-29, 2014

Semiactive Virtual Control Method for Robots with Regenerative Energy-Storing Joints ⋆

Hanz Richter * **Dan Simon** ** **Antonie van den Bogert** ***

* *Cleveland State University, Mechanical Engineering (e-mail: h.richter@.csuohio.edu).*
** *Cleveland State University,Electrical and Computer Engineering*
*** *Cleveland State University, Mechanical Engineering*

Abstract: A framework for modeling and control is introduced for robotic manipulators with a number of energetically self-contained semiactive joints. The control approach consists of three steps. First, a virtual control design is conducted by any suitable means, assuming a fully-actuated system. Then, virtual control inputs are matched by a parameter modulation law. Finally, the storage dynamics are shaped using design parameters. Storage dynamics coincide with the system's internal dynamics under exact virtual control matching. An internal energy balance equation and associated self-powered operation condition are given for the semiactive joints. This condition is a structural characteristic of the system and independent of the control law. Moreover, the internal energy balance equation is independent of the energy storage parameter (capacitance), which adds flexibility to the approach. An external energy balance equation is also given that can be used to calculate the work required from the active joints. A simulation example using a 3-dof prosthesis test robot illustrates the concepts.

Keywords: robot control, energy regeneration, semiactive control, ultracapacitors, powered prosthetics.

1. INTRODUCTION

Energy regeneration technologies have regained attention in recent years as higher efficiency standards are sought for vehicles, autonomous robots, biomedical devices and industrial systems. The field of powered prosthetics is not an exception, where range is as important as human-like motion control. Motion, force and impedance control algorithms for robotic manipulators have been advanced for several decades, but analysis and design methods addressing dynamic interaction with on-board energy storage systems are relatively scant. Control with energy regeneration has always been a topic of interest in the field of prosthetics, which included pioneering work conducted in the 1980's by an MIT group (Hunter (1981); Tabor (1988); Seth (1987)) and more recent advances, for instance Hitt et al. (2009); Lawson et al. (2011); Sup et al. (2008) and van den Bogert et al. (2012), where simultaneous control and energy regeneration are achieved for a hydraulic knee actuator. Unal et al. (2012) developed a fully-passive transfemoral prostheses which extracts energy from the knee and transfers it to the ankle. Energy recuperation in industrial robotics systems has the potential to produce impressive economic advantages (Rankis et al. (2013)). Most published work concerning control with regeneration is based on simulations of specific designs or evaluations of practical prototypes. The work summarized in this paper takes a few steps in the direction of generality, introducing a flexible framework within which analysis, design and optimization can be conducted with good flexibility. Aside from a generic physical model, we propose a control strategy which allows to separate the motion control task (understood as trajectory, force, hybrid force/trajectory or impedance control) from the energy storage dynamics. The bond graph approach is used to provide insight about power flows and dynamics and to maintain generality and modularity. This way, robots with electromechanical or hydraulic joints, and electric or hydraulic energy conversion, modulation and storage can be unified in a single approach. The framework and control concept can also be extended to systems other than robotic where bi-directional power flow may be controlled, like vehicles and smart structures with piezoelectric transducers. This paper develops the electromechanical case only, that is, mechanical transmissions and electric motors are attached to all joints. Semiactive joint mechanisms contain a storage element (an ultracapacitor) and power conversion and modulation electronics. Ultracapacitors are highly-efficient devices increasingly being used in conjunction with batteries (or even as the single storage medium) in regenerative power systems (Conway (1999)). Ultracapacitors can be charged and discharged at similar (fast) rates, unlike batteries, which cannot be charged fast enough to match the rate of regenerative energy flow found in many applications. Ultracapacitors also have the advantages of being lightweight, inexpensive and durable.

⋆ Work supported by the National Science Foundation, Grant #1344954 and the Wright Center for Sensor Systems Engineering through the state of Ohio, Third Frontier Program.

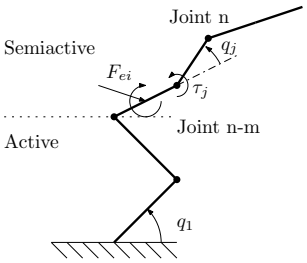

Fig. 1. Robotic manipulator configuration.

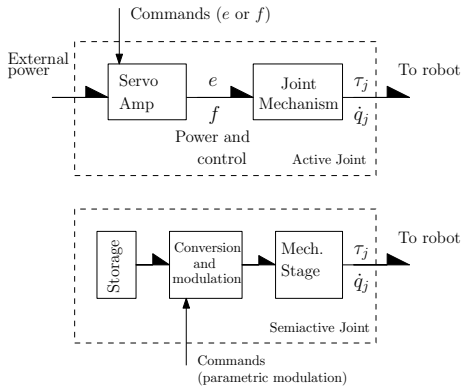

Fig. 2. Schematic of active and semi-active joints.

2. MATHEMATICAL MODEL AND ASSUMPTIONS

The general arrangement consists of a robotic manipulator in an open-chain configuration having n degrees of freedom (joints). The first $n-m$ joints, including the base joint, are assumed to be fully-actuated, while the remaining m joints are semi-actuated, as shown in Fig. 1. Torque (or force, as applicable) is applied to rotary (prismatic) joints by a set of joint mechanisms (JM) attached to each joint. A *fully-actuated* joint mechanism (JM) exchanges mechanical power with the robot and with an external source. Power transfer from the external source is described by a pair of variables, effort and flow, whose product equals power. The force or moment output of a fully-actuated JM is controlled by commanding changes to one of the 2 power variables. For example, a fully-actuated JM with an electric motor is controlled by commanding either the motor voltage or current. In contrast, a *semiactive* JM only exchanges mechanical power with the robot. Semiactive JMs are composed only of ideal power converters, energy-storing and dissipative elements. Moreover, the output of a semiactive JM is controlled by modulating of one or more of its internal parameters, and modulation itself is assumed to require zero or negligible power. For example, the power required to adjust the duty cycle of an electronic converter is considerably smaller than load power. The bond graph formalism is used to model JMs without regard to the nature of their physical components (electrical, mechanical, hydraulic, etc.). A half-arrow indicates bidirectional power flow, while a full-arrow indicates information flow at zero power. Following customary conventions, power flows in the direction of the half-arrow when the product of the effort and flow variables associated to that bond is positive. Figure 2 illustrates the above concepts. Standard dynamic equations are assumed for the robotic manipulator alone (without JMs), that is:

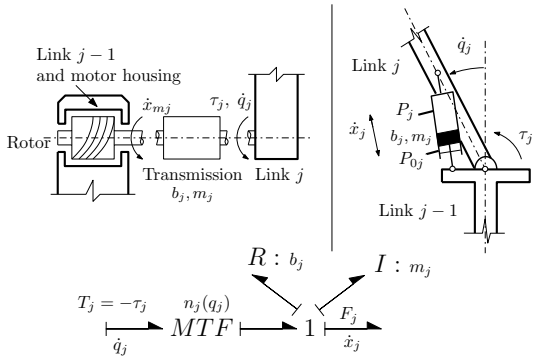

Fig. 3. Schematic of inline (electromechanical example) and crank-slider (hydraulic example) joints.

$$D(q)\ddot{q} + C^o(q,\dot{q})\dot{q} + \mathcal{R}^o(q,\dot{q}) + g^o(q) = \tau \tag{1}$$

where q is an $n-$vector of joint displacements, $D(q)$ is the inertia matrix, $C^o(q,\dot{q})$ is a matrix accounting for centripetal and Coriolis effects, $\mathcal{R}^o(q,\dot{q})$ is a general damping term, $g^o(q)$ is the gravity vector and τ is the vector of forces or moments applied at the joints. The JM is assumed to be a one-port passive system, where the port variables are τ_j and $\dot{q}_j$. Each JM contains a purely mechanical stage composed of a transmission element, inertial elements and frictional elements. The output port of this stage is connected to a power conversion element such as an electric motor/generator, or a hydraulic cylinder or pump. An energy storage device, inertial and dissipative elements and additional passive elements intended for modulating control are connected after the power conversion element. The bond graph of Fig. 3 (bottom) captures a wide class of mechanical input stages. Transmissions such as gear trains and crank-slider mechanisms are readily incorporated after finding the applicable velocity ratio function $n(q_j)$. For instance, $n(q_j)$ for a gear train is some constant, and $n(q_j)$ for the slider-crank mechanism depends on $\cos(q_j)$. It is assumed that $n(q_j)$ is a non-singular kinematic transformation between $\dot{q}_j$ and the input speed of the power conversion element. Without loss of generality, we assume $n(q_j) > 0$ for all q_j in the design range of the JM. The inertial and frictional elements m_j and b_j are assumed to be quantities reflected to the output of the transmission. In the hydraulic piston example of Fig. 3, m_j is the mass of the piston, while b_j is a viscous friction coefficient associated with linear motion of the piston. In the gear transmission example, m_j and b_j are the moment of inertia and viscous damping of the gear train and motor reflected to the motor shaft side.

In what follows, it is then assumed that the mechanical stage of the JM can be described by the bond graph of Fig. 3. It is convenient to absorb the inertial, workless and damping terms of the mechanical stage into the manipulator dynamics. T_j is found by conventional methods or from the bond graph as

$$\begin{aligned} -T_j = \tau_j = &-m_j n_j^2(q_j)\ddot{q}_j - b n_j^2(q_j)\dot{q}_j \\ &-m_j n_j(q_j)\frac{dn_j(q_j)}{dq_j}\dot{q}_j^2 - n_j(q_j)F_j \end{aligned} \tag{2}$$

while robot dynamics for the j-th coordinate are given by

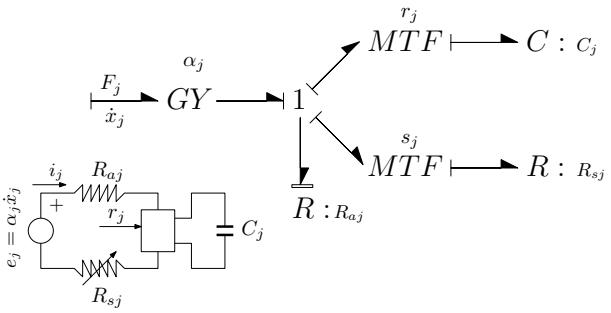

Fig. 4. Schematic and bond graph of conversion, modulation and storage elements in the electromechanical semiactive JM

$$\sum_{i=1}^{n} D_{ji}(q_i)\ddot{q}_j + \sum_{i=1}^{n} C_{ji}(q_i, \dot{q}_i)\dot{q}_j + \mathcal{R}_j + g_j(q_j) = \tau_j \quad (3)$$

The inertial and frictional terms in Eq. 2 are directly incorporated into robot dynamics by adding $m_j n_j^2(q_j)$ and $b n_j^2(q_j)\dot{q}_j$ to the j-th diagonal entries of $D(q)$ and $\mathcal{R}_j$, respectively. The quadratic term is factored as $m_j n_j(q_j)\frac{dn_j(q_j)}{dq_j}\dot{q}_j^2 = c_j(q_j, \dot{q}_j)\dot{q}_j$, and $c_j(q_j, \dot{q}_j)$ is added to the j-th diagonal entry of $C(q, \dot{q})$. This defines a set of augmented dynamic matrices $M(q)$, $C(q)$, $\mathcal{R}$ and $g(q) = g^o(q)$. It is readily shown that $M(q)$ and $C(q, \dot{q})$ retain the fundamental properties of passivity, skew-symmetry and linear parameterization (Spong et al. (2006)). Note that the nomenclature introduces opposite signs for the torque applied to the robotic link and that applied to the joint mechanism, that is, $\tau_j = -T_j$. Accordingly, $T_j\dot{q}_j > 0$ indicates that mechanical energy is being transferred to the JM at the expense of robot energy, that is, $\tau_j\dot{q}_j$ will be negative (regeneration mode). Conversely, $T_j\dot{q}_j < 0$ corresponds to the driving mode.

2.1 Conversion, Modulation and Storage

The output of the mechanical stage is connected to a primary power conversion element. Converted energy may be hydraulic, electric or again mechanical. Energy transfer from the converter to a compatible storage element (accumulator, capacitor or flywheel) is modulated by the converter itself or by additional elements. In this paper we focus on a DC motor/generator as the primary converter and an ultracapacitor as the storage medium. An ideal element known in the bond graph terminology as *modulated transformer* is installed between the DC machine and the ultracapacitor to control energy flow to and from the storage element through parameter r_j. The proposed approach relies on the availability of a four-quadrant (4Q) or bidirectional power modulation devices. Commercial electronic converters realize this function, and a hydraulic version of a 4Q transformer has also been developed (Vael et al. (2001)). Figure 4 shows the arrangement considered in this paper. The motor armature resistance is R_{aj}, while the additional R_{sj} is added intentionally. An additional transformer modulated by s_j controls power flow into the additional series resistance, and it may be just a switch. Thus, r_j and s_j are assumed to be adjustable at will (at least in some interval). The ideal transformers instantaneously enact any commanded ratio between the effort variables at the ports. Since they are power-conserving, the reciprocal ratio must hold for the flow variables. Deviations from ideality are discussed in the conclusions section. From Fig. 4, the following port relationship can be obtained for the conversion stage of the electromechanical JM:

$$F_j = \frac{\alpha_j}{R_j}\left(a_j\dot{q}_j - \frac{r_j}{C_j}y_j\right) \quad (4)$$

where α_j is the torque (and back-emf) constant of the DC machine, $a_j = \alpha_j n_j(q_j)$, $R_j = R_{aj} + s_j^2 R_{sj}$, y_j is the electrical charge and C_j is the capacitance.

2.2 Augmented Robot Model and Virtual Control

Combining Eqs. 2 and 4, and absorbing all inertial, dissipation and workless terms of the JM into the baseline robot dynamics of Eq.1 results in the following augmented model:

$$M(q)\ddot{q} + C(q, \dot{q})\dot{q} + \mathcal{R} + g = u \quad (5)$$

where $u_j = \tau_j$ (actively controlled) for $j = 1, 2..n-m$ and $u_j = \frac{a_j r_j}{C_j R_j}y_j$ for $j = n-m+1, n-m+2, ...n$. The mass matrix satisfies $M_{ij} = D_{ij}$ for all $i \neq j$ and $M_{jj} = D_{jj} + m_j n_j^2(q_j)\ddot{q}_j$ for $j = n-m+1, n-m+2, ...n$. The Coriolis matrix satisfies $C_{ij} = C_{ij}^o$ for all $i \neq j$ and $C_{jj} = C_{jj}^o + m_j n_j(q_j)\frac{dn_j(q_j)}{dq_j}\dot{q}_j$ for $j = n-m+1, n-m+2, ...n$. The dissipation term satisfies $\mathcal{R}_j = \mathcal{R}_j^o$ for $j = 1, 2, ...n-m$ and $\mathcal{R}_j = \mathcal{R}_j^o + (b_j n_j^2(q_j)\dot{q}_j + \frac{a_j^2}{R_j})\dot{q}_j$ for $j = n-m+1, n-m+2, ...n$. The gravity term is unaffected, $g = g^o$. The linear parameterization property assures that Eq. 5 can always be factored as

$$M(q)\ddot{q} + C(q, \dot{q})\dot{q} + \mathcal{R} + g = Y(q, \dot{q}, \ddot{q})\Theta \quad (6)$$

where Y is a regressor matrix which is independent of parameters and Θ is a parameter vector. The dimensions of Θ depend on the characteristics of the manipulator.

3. CONTROL STRATEGY

Vector u in Eq. 5 is divided into $n-m$ active inputs $u_j = \tau_j$ and m terms of the form $u_j = \frac{a_j r_j}{C_j R_j}y_j$. The latter cannot be controlled directly, but changed by modulation parameters r_j and s_j ($R_j = R_j(s_j)$), and will be termed *virtual control*, in the same spirit as the backstepping approach (Khalil (2001)). Unlike backstepping, which is better suited to underactuated systems (where there is no direct authority over the virtual control) the semiactive case allows exact matching of the virtual control via parameter modulation. That is, if $u_j = \tau_j^d$ arises from some predetermined control law, we simply choose r_j and s_j so that $\tau_j^d = \frac{a_j r_j}{C_j R_j}y_j$. This will be termed *exact virtual control matching*. Thus, the control strategy can be viewed as a 3-step process: first a *virtual design* is completed for the augmented model of Eq. 5, assuming full authority over u. The virtual design is assumed to meet some control objectives: stability, robustness, regulation, tracking, and so forth. This step has been essentially solved after several decades of research and many methodologies are available, ranging from SISO PD methods, MIMO Lyapunov-based robust and adaptive

controls, optimal control, neural/fuzzy control and others. The second step is the virtual control matching for the semiactive joints. The third step, discussed below, is to shape the internal dynamics that arise as a consequence of exact matching. Provided exact matching is possible, the approach offers several advantages, starting with the propagation of all properties of the virtual design (stability, robustness, tracking performance) to the final system. Also, no differentiation of the virtual control is required, as it happens with backstepping, and the characteristic "explosion of terms" (Swaroop et al. (2000)) is absent. Further, the resulting internal dynamics have a clear energy interpretation.

3.1 Virtual Control Matching: Electromechanical JM

If τ_j^d is the desired virtual control for the j-th semiactive JM, the modulation law for exact matching is simply

$$r_j = \frac{\tau_j^d R_j}{a_j \frac{y_j}{C_j}} \tag{7}$$

Noting that $\frac{y_j}{C_j}$ is the capacitor voltage, this is termed the *voltage form* of the matching law. It is well-defined as long as the capacitor is not fully discharged. As with batteries, a lower voltage threshold indicates that the storage element must be recharged and operation is stopped, thus $y_j = 0$ will not be encountered in practice. Whether y_j approaches zero, grows or oscillates around an average is discussed below. If τ_j^d contains an explicit cancellation of the damping-like term $\frac{a_j^2}{R_j}\dot{q}_j$, that is,

$$\tau_j^d = \tau_j^c + \frac{a_j^2}{R_j}\dot{q}_j \tag{8}$$

where τ_j^c is some designed virtual control, it can be shown that the matching law becomes

$$r_j = -\frac{a_j}{\tau_j^c}\dot{y}_j \tag{9}$$

which is termed the *current form* of the matching law. It becomes singular whenever the computed control crosses zero. For this reason, even when τ_j^d is of the form of Eq. 8, the voltage form should be used.

3.2 Internal Dynamics and Energy Balance

The exact matching law of Eqs. 7 and 9 do not change the number of state variables in the overall system composed of the base manipulator and joints. Each semiactive joint contributes a state variable, namely the charge in the storage element. The dynamics of this variable under exact virtual matching are of fundamental importance, since they correspond to the *internal dynamics* of the overall closed-loop system. Assuming τ_j^d is of the form of Eq. 8, direct substitution shows that the following nonlinear differential equation holds for y_j:

$$\frac{y_j \dot{y}_j}{C_j} = -\tau_j^c \dot{q}_j - \frac{R_j}{a_j^2}(\tau_j^c)^2 \tag{10}$$

The term on the left hand side is an exact integral and corresponds to the rate of energy flowing into the storage element. Integration between times t_1 and t_2 yields the *internal energy balance* equation:

$$\frac{y_j^2(t_2) - y_j^2(t_1)}{2C_j} = \Delta E_{sj} = -\int_{t_1}^{t_2} (\tau_j^c \dot{q}_j + \frac{R_j}{a_j^2}(\tau_j^c)^2) dt \tag{11}$$

Further, it can be shown by that the second term under the integral sign equals the "i^2R" or Joule power loss in the resistive elements of the JM. Thus, ΔE_{sj} will be zero between any two times if the work done by the virtual control $-\tau_j^c = T_j$ (the term "virtual work" should be avoided in this context) balances electric dissipation in the JM. Often, trajectories to be tracked are periodic. Suppose the integrand of Eq. 11 is a periodic function of time, and ΔE_{sj} is zero over a cycle. Further, suppose $y_j > 0$ during the cycle. Then, the semiactive joint is said to be in *self-powered operation* (SPO condition). Although the SPO condition cannot be exactly maintained in practice, it is of theoretical importance. If SPO does not hold, the capacitor will either discharge eventually, or will continue to charge until its practical operating limits are exceeded. Strictly speaking, lack of SPO indicates unbounded internal dynamics. Despite of this, it is possible to affect ΔE_{sj} by means of design choices (system parameters), control gains and even the reference trajectories in path planning problems. Two practical situations arise: i. parameters are chosen so that $\Delta E_{sj} < -\eta < 0$ holds, where loss rate η determines the period of time where the system can operate before a recharge is needed; and, ii. parameters are chosen so that $\Delta E_{sj} > \eta > 0$ holds, with η dictating the time to reach a maximum allowable stored energy. In this case, an outer-loop supervisory strategy can use s_j to increase series resistance once the stored energy crosses an upper threshold, so that the energy starts to decrease. The additional series resistance is removed upon crossing a lower threshold, much like in a thermostat control system. This justifies the inclusion of the additional resistance and a modulating switch in the JM model. Note that this strategy would effectively create a hybrid system. It is well-known that unstable systems (and collections of unstable systems) can be stabilized by appropriate switching strategies. For the electromechanical JM, it is remarkable that the virtual control design step and internal energy balance equation are independent of the storage parameter C_j. This implies that C_j can be chosen independently to address desired operating time horizons and to bound r_j. Note that the use of semiactive JMs affords a much simpler and flexible approach to the control problem of robots with electrically-actuated joints than has been considered with backstepping-based methods, for instance in Su and Stepanenko (1997).

3.3 SPO Condition and Linear Parameterization

More insight into the feasibility of the SPO condition can be derived if some information is available concerning the virtual control objectives and the kind of virtual law in use. The inverse dynamics law (also known as computed torque law) used with the linear parameterization property is particularly illustrative. Let the virtual control be determined by

$$u = Ma + C\dot{q} + \mathcal{R} + g \tag{12}$$

where $a = \ddot{q}^d - K_0\tilde{q} - K_1\dot{\tilde{q}}$ is the virtual acceleration and $\tilde{q} = q - q^d$ is the tracking error. This feedback linearization law inverts dynamics and transforms Eq. 5 into a set of n decoupled double integrators. The virtual acceleration is chosen so that the double integrator plants track the reference trajectories. A PD law is used in this case. By the linear parameterization property, u may be expressed as

$$u = Y_a(q, \dot{q}, a)\Theta \tag{13}$$

where Y_a is the regressor Y with virtual accelerations in place of actual ones. If Y_{aj} denotes the j-th row of Y_a for a semiactive joint, the virtual control law has the form $u_j = \tau_j^c = Y_{aj}\Theta$. The internal energy balance equation becomes

$$\Delta E_{sj} = -\int (Y_{aj}\Theta\dot{q}_j + \frac{R_j}{a_j^2}\Theta^T Y_{aj}^T Y_{aj}\Theta)dt \tag{14}$$

Note that the above equation is quadratic in parameters, which represents an advantage when concurrent optimal design and control problems are considered. Many control laws, including inverse dynamics under nominal conditions, will lead to asymptotic tracking of trajectories. Then, Y_{aj} will converge to $Y_{jd} = Y_j(q^d, \dot{q}^d, \ddot{q}^d)$, since $\tilde{q}$ will approach zero. This observation motivates another self-powered operation condition, termed *ideal* SPO, or ISPO:

$$0 = \Delta E_{sj} = -\int (Y_{jd}\Theta\dot{q}_j^d + \frac{R_j}{a_j^2}\Theta^T Y_{jd}^T Y_{jd}\Theta)dt \tag{15}$$

The ISPO condition reflects the structure of the system and is independent of the control input, but may hold for some trajectories and not for others.

3.4 External Energy Balance

The energy balance of Eq. 11 is JM-centric. The amount of work required from the active joints to maintain SPO is of importance, particularly in prosthetics. In a human-prosthesis system, active joints are functional human joints, and its is important that a prosthesis does not require an excessive amount of power from its wearer. A somewhat long derivation shows that the work of the active joints is given by

$$W_{ACT} = \sum_{j=1}^{j=n-m} \int \tau_j\dot{q}_j dt = \tag{16}$$

$$\sum_{j=n-m+1}^{j=n} \int \Delta E_{sj}dt + \Delta E_m^T + \sigma_m^T + \sum_{j=n-m+1}^{j=n} \int \frac{R_j}{a_j^2}(\tau_j^c)^d dt$$

where ΔE_m^T is the change in total (robot+JMs) mechanical energy, σ_m^T is the total mechanical energy dissipation (friction work) and the last term equals σ_e^T, the total Joule loss in the JM resistors. This equation only confirms the conservation of energy law, but is useful to compute W_{ACT}.

4. EXAMPLE

As an example, consider a 3-link robot with a prismatic-revolute-revolute joint configuration, as shown in Figure 5.

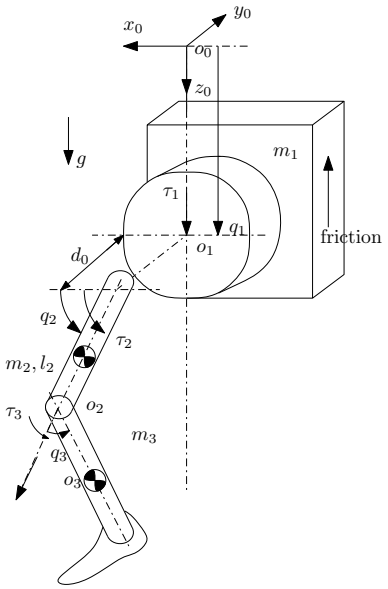

Fig. 5. Schematic of 3-dof Prosthesis Test Robot

The model is a simplification of an actual prosthesis-testing machine (Richter and Simon (2014)), where the vertical axis emulates human hip oscillations, and two rotational axes emulate the thigh and the knee. Above-knee prosthesis prototypes are attached to the machine and hip and thigh reference trajectories are tracked by a control system, as the prosthesis walks on a built-in treadmill. The performance of the prosthetic knee and its control system are then evaluated. In this example, we consider the first two joints to be actively-controlled, while a semiactive electromechanical JM is used for the knee. Actuator dynamics have been omitted for the two active joints for simplicity, assuming that direct force/torque control inputs are applied. The inertial and friction constants of the active joints in the simulation include actuator contributions, however. The ultracapacitor has $C_3 = 500$F and is rated at 16V. No external force is considered in this example. Following the coordinate system shown in Figure 5, the augmented robotic equations of Eq. 1 can be linearly parameterized as

$$M\ddot{q} + C\dot{q} + g + \mathcal{R} = Y(q, \dot{q}, \ddot{q})\Theta = u$$

where the regressor and parameter vector are shown in the appendix, along with parameter values. Note that all JM friction and inertia terms are reflected in the augmented model. The first 2 components of u are the active control force and torque, and the third is the virtual input $a_3 r_3 y_3/(R_3 C_3)$. Inverse dynamics is used for the virtual design, with gains K_0=diag(2,3,5) and K_1=diag(1,5,5). Parameters were set to correspond to the actual machine, while values for JM parameters are within the ranges of commercially-available devices. Two values of the gear ratio n_3 were chosen for the simulation study, showing positive and negative ΔE_{s3} trends. Figure 6 shows the three tracking reference trajectories reflecting normal human walking (van den Bogert et al. (2012)). These trajectories are periodic. For the parameters used in the study, self-powered operation of the semiactive joint holds at $n_3 = 23.26$. A plot of ΔE_{s3} based on Eq. 15 is shown. Note that the average energy in a cycle is zero. Figure 7 shows the tracking errors, which are the same

regardless of n_3 due to the exact virtual control matching and inverse dynamics. Modulating parameter r_3, however, varies according to n_3. Note that it remains bounded and that negative and positive values are used. Figure 8 shows the control input histories. Active control histories are the same regardless of n_3, however u_3 differs, since it cancels JM reflected damping, which depends on n_3. The capacitor voltage is also shown, displaying a slow charging trend for n_3 above the self-powered value and a slow discharging trend for n_3 below this value. Note that the work done by the active inputs is the same regardless of n_3, since control forces are the same and asymptotic tracking of the same reference velocities is achieved. Because of this, mechanical dissipation is also equal. Finally, the change of total mechanical energy in a cycle is zero. How is it then possible that in one case the capacitor accumulates charge? As shown in Table 1, the electric dissipation is smaller for $n_3 = 30$. In an actual design problem, if a positive ΔE_{s3} "trim" occurs for the nominal trajectories and expected external forces, an outer supervisory loop that adds series resistance can be used. If the opposite occurs, the capacitor must be sized to provide the desired semiactive operation time. The results of this paper can be used to predict the discharge time.

Table 1. Energy Balance Figures (Joules)

n_3	W_{ACT}	ΔE_{s3}	σ_m^T	σ_e^T	ΔE_m^T
20	65.666	-5.6136	50.6722	20.5989	0.0091
30	65.666	5.8303	50.6722	9.1551	0.0091

5. REMARKS

The semiactive JM hardware presented here is also capable of operating in active mode. That is, the capacitor can be placed offline and the converter fed by an external source such as a battery. The virtual control law is then enforced as done traditionally, via motor voltage or current commands and the modulation portion is deactivated. Switching a JM from active to semiactive mode would be governed by a high-level supervisory strategy determined from optimality criteria and constraints pertaining to the particular case. The conversion and modulation elements considered for the JMs were modeled as power-neutral, proportional and devoid of dynamics. The first two restrictions are not difficult to handle, as additional resistance can be used to model non-ideal conversion efficiency and static nonlinearity may be inverted. First-order models were used for the JMs, which makes exact virtual matching rather simple. Several factors can bring additional dynamics, such as motor inductance or modulating element dynamics. If the states of the JM are measurable and available for feedback, it seems possible to find appropriate matching laws for higher-order JM models, but this requires further study. The analysis shows some similarities with AC circuits, where resistive power (typically stated in W) plays the role of dissipation, and reactive power (typically stated in VA) plays the role of stored energy flow. Of course, in regenerative systems one wants to minimize dissipation, but dissipation may also be necessary to achieve accurate tracking, as the example shows. The additional resistance was placed in series, but a parallel arrangement or other topologies can be considered under the same framework. Electric charge transfer between the

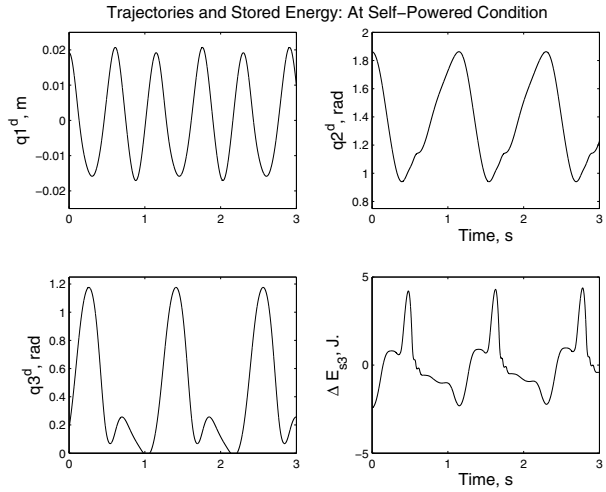

Fig. 6. Simulation results: Reference trajectories and ISPO condition.

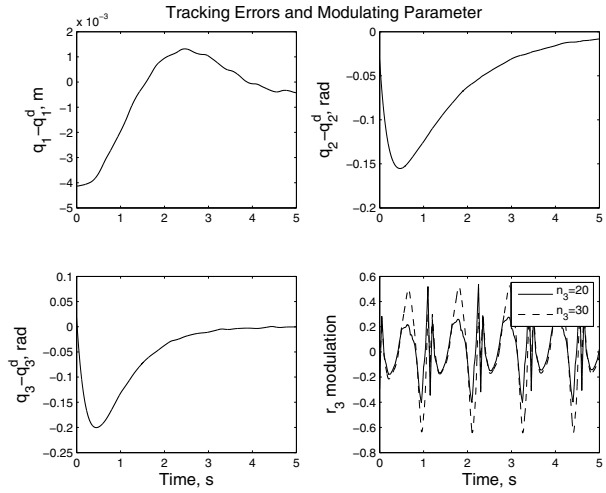

Fig. 7. Simulation results: Tracking errors and modulation parameter

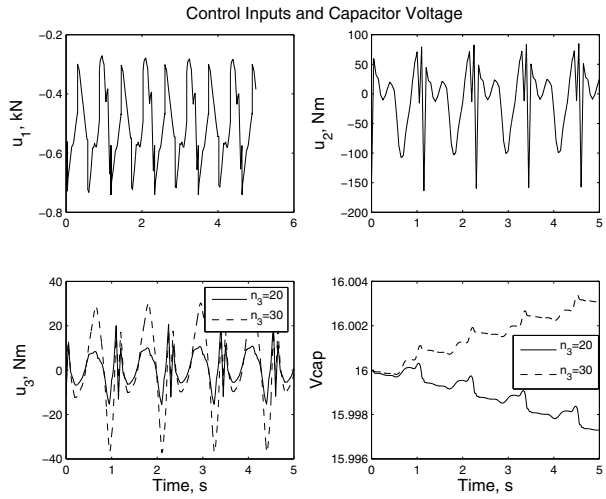

Fig. 8. Simulation results: Control inputs and capacitor voltage

capacitors of different JMs has not been enabled, but one can envision replacing the additional series resistance by another modulated converter connecting the JM to a common rail where all other JMs are also connected in a ring topology, which can include a backup battery. The example shows that the SPO and ISPO conditions hold for the robot under consideration, but further study is required concerning the feasibility of the SPO conditions for other configurations. Although electromechanical JMs were considered, the three basic steps of the approach can be followed to arrive at appropriate energy balance equations and SPO conditions for hydraulic systems with accumulators as storage elements or mechanical systems with flywheels, springs or potential energy storage mechanisms, as may be found in spacecraft and exercise/rehabilitation machines.

REFERENCES

Conway, B. (1999). *Electrochemical Supercapacitors: Scientific Fundamentals and Technological Applications*. Springer.

Hitt, J. et al. (2009). Robotic transtibial prosthesis with biomechanical energy regeneration. *Industrial Robot: An International Journal*, 36(5), 441–447.

Hunter, B. (1981). *Design of a Self-Contained Active, Regenerative, Computer-Controlled Above-Knee Prosthesis*. Master's thesis, Massachussetts Institute of Technology.

Khalil, H. (2001). *Nonlinear Systems*. Prentice-Hall.

Lawson, B., Varol, H., and Goldfarb, M. (2011). Standing stability enhancement with an intelligent powered transfemoral prosthesis. *IEEE Trans. Biomed. Eng.*, 58(9), 2617–2624.

Rankis, I., Meike, D., and Šenfelds, A. (2013). Utilization of regeneration energy in industrial robots system. *Power and Electrical Engineering, Scientific Journal of the Riga Technical University*, 31, 95–100.

Richter, H. and Simon, D. (2014). Robust tracking control of a prosthesis test robot. *ASME Journal of Dynamic Systems, Measurements and Control*, 136(3). doi:10.1115/1.4026342.

Seth, B. (1987). *Energy Regeneration and its Application to Active Above-Knee Prostheses*. Ph.D. thesis, Massachussetts Institute of Technology.

Spong, M., Hutchinson, S., and Vidyasagar, M. (2006). *Robot Modeling and Control*. Wiley.

Su, C.Y. and Stepanenko, Y. (1997). Backstepping-based hybrid adaptive control of robot manipulators including actuator dynamics. *Int. Journal of Adaptive Control and Signal Processing*, 11, 141–153.

Sup, F., Bohara, A., and Goldfarb, M. (2008). Design and control of a powered transfemoral prosthesis. *International Journal of Robotics Research*, 27(2), 263–273.

Swaroop, D. et al. (2000). Dynamic surface control for a class of nonlinear systems. *IEEE Trans. Aut. Control.*, 45(10), 1893–1899.

Tabor, K. (1988). *The Real-Time Digital Control of a Regenerative Above-Knee Prosthesis*. Master's thesis, Massachussetts Institute of Technology.

Unal, R. et al. (2012). Towards a fully passive transfemoral prosthesis for normal walking. In *Proc. IEEE. RAS EMBS Int. Conf. Biomed. Robot. Biomechatron.*, 1949–1954.

Vael, G., Achten, P., and Zhao, F. (2001). The Innas hydraulic transformer: The key to the hydrostatic common pressure rail. In *SAE Technical Paper 2000-01-2561*. doi:10.4271/2000-01-2561.

van den Bogert, A., Samorezov, S., Davis, B., and Smith, W. (2012). Modeling and optimal control of an energy-storing prosthetic knee. *ASME J. Biomechanical Engineering*, 134(5), 051007.

Appendix A. REGRESSOR AND PARAMETERS: SIMULATION EXAMPLE

Shorthand used for trigonometric functions: $\cos(q_1) = c_1$, $\sin(q_2 + q_3) = s_{23}$, etc.

$$Y_{11} = \ddot{q}_1 - g; \;\; Y_{12} = \ddot{q}_2 c_2 - \dot{q}_2^2 s_2$$
$$Y_{13} = -s_{23}(\dot{q}_2 + \dot{q}_3)^2 + c_{23}(\ddot{q}_2 + \ddot{q}_3)$$
$$Y_{14} = Y_{15} = Y_{16} = Y_{17} = Y_{19} = 0; \;\; Y_{18} = \text{sign}(\dot{q}_1)$$
$$Y_{21} = 0; \;\; Y_{22} = (\ddot{q}_1 - g)c_2; \;\; Y_{23} = (\ddot{q}_1 - g)c_{23}$$
$$Y_{24} = \ddot{q}_2; \;\; Y_{25} = (2\ddot{q}_2 + \ddot{q}_3)c_3 - (2\dot{q}_2 + \dot{q}_3)\dot{q}_3 s_3$$
$$Y_{26} = \ddot{q}_3; \;\; Y_{27} = \dot{q}_2; \;\; Y_{28} = Y_{29} = 0$$
$$Y_{31} = Y_{32} = Y_{34} = Y_{37} = Y_{38} = 0$$
$$Y_{33} = Y_{23}; \;\; Y_{35} = s_3 \dot{q}_2^2 + \ddot{q}_2 c_3$$
$$Y_{36} = \ddot{q}_2 + \ddot{q}_3; \;\; Y_{39} = \dot{q}_3$$

Parameter Vector Elements:
$\Theta_1 = m_1 + m_2 + m_3'$; $\Theta_2 = (m_3 + m_2)l_2 + m_2 c_2$; $\Theta_3 = c_3 m_3$
$\Theta_4 = I_{2z} + I_{3z} + c_2^2 m_2 + c_3^2 m_3 + l_2^2(m_2 + m_3) + 2c_2 l_2 m_2$
$\Theta_5 = l_2 m_3 c_3$; $\Theta_6 = m_3 c_3^2 + I_{3z}$; $\Theta_7 = b$; $\Theta_8 = f$
$\Theta_9 = n_3^2 b_3$

Robot Parameters:
Link masses: m_1, m_2, m_3', kg; link lengths: l_2, l_3, m
CM distances from joints: c_2, c_3, m
Link CM inertias: I_{2z}, I_{3z}, kg-m^2
Viscous damping, joint 2: b, N-m-s.
Coulomb friction, joint 1: f, N

Table A.1. Simulation Parameters (Robot)

m_1	m_2	$m_3^{'}$	I_{2z}	I_{3z}
40.6	8.57	2.29	0.435	0.0618
l_2	c_2	c_3	f	b
0.425	0.0900	0.0320	83.3	9.75

Semiactive JM Parameters:
DC machine torque constant: α_3, N-m/A
DC machine series resistance: R_{a3}, Ω
Additional series resistance: R_{s3}, Ω
Viscous damping (motor and gears, reflected to motor side) : b_3, N-m-s
Rotary inertia (motor and gears, reflected to motor side) : $m_3^{'}$, kg-m^2
Gear ratio: n_3, variable
Ultracapacitor capacitance, C_3, F.
Ultracapacitor charge capacity, $\bar{y}_3$, C

Table A.2. Simulation Parameters (Semiactive JM)

α_3	R_{a3}	R_{s3}	b_3	$m_3^{'}$	C_3	$\bar{y}_3$
0.06	0.5	0	0	1×10^{-5}	500	8000